Current Research in Green and Sustainable Chemistry 9 (2024) 100425

Contents lists available at ScienceDirect

Current Research in Green and Sustainable Chemistry

journal homepage: www.elsevier.com/journals/current-research-in-green-and-sustainable-chemistry/2666-0865

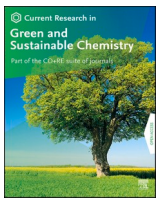

Sustainable ambient pressure-dried silica aerogel from waste glass

M. Borzova *, K. Schollbach, F. Gauvin, H.J.H. Brouwers

Department of the Built Environment, Eindhoven University of Technology, P. O. Box 513, 5600 MB, Eindhoven, the Netherlands

ARTICLE INFO

Keywords:
Silica aerogel
Thermal conductivity
Insulation material
Evaporative drying
Glass
Waste management
Water glass

ABSTRACT

Silica aerogels are outstanding insulation materials, and applying them as building insulation could significantly enhance the energy efficiency of dwellings. However, the current high price of aerogels hinders their use on large scales, in part due to the embedded costs of production such as raw materials and their energy-intensive drying process. This study proposes a method relying on the upcycling of waste mixed fine soda lime glass as a silica source for subsequent aerogel synthesis via ambient pressure drying (APD). The optimal conditions for the dissolution of silica from waste glass were found to be a 24-h reaction with a 4 M NaOH solution under 80 °C and a liquid-to-solid ratio of 10. The investigation of silica dissolution considers the balance between the yield of silica and the practical scalability. The resulting aerogel is hydrophobic, has a thermal conductivity of 26 mW m^{-1} K^{-1}, a specific surface area of 608 m^2 g^{-1}, and a density of 121 kg/m^3. These properties are comparable to commercial aerogel, and to a reference aerogel made from commercial sodium silicate. Additionally, the heat treatment of aerogel at 500 °C for 4 h further improved its properties, suggesting a potential for targeted property enhancements.

1. Introduction

In the EU, 27.4 % of total energy was consumed by households, of which 62.8 % was used towards heating in 2020 [1]. In the Netherlands, approximately 3.7 million poorly insulated homes (energy labels C to G) need to be renovated at a rapid pace. Applying changes to achieve an energy label of A++ can reduce heating demand by 60 %, which is not only important in terms of environmental benefits but is also crucial for residents as gas prices are increasing drastically. By 2050, 7 million homes are planned to be independent of natural gas use in the Netherlands, therefore a solution for renovation to increase energy efficiency is urgently needed [2]. Many Dutch houses have an air-filled wall cavity that can be filled with an insulation material. Unlike aerogel, currently available affordable products cannot achieve the A++ energy label as meeting such standards would demand a greater volume of insulation material than the existing wall cavities can accommodate. This issue can only be resolved by either compromising the insulation quality or building a new façade thus increasing the available space for insulation.

Silica aerogel is an ultra-light highly porous material with extremely low density and high specific surface area. Additionally, it is inherently flame retardant, which makes it an outstanding insulation material [3]. Silica aerogels have the lowest thermal conductivity (10–20 mW m^{-1} K^{-1}) when compared with traditional insulation materials such as mineral wool (38–40 mW m^{-1} K^{-1}) and EPS (35 mW m^{-1} K^{-1}) [4,5]. Prior research found that aerogel-insulated single-family houses consume on average 20.9 % less kWh compared to other commonly used insulation materials, given a thickness of 1.3 cm [6]. Most commercial silica aerogels are produced using waterglass, tetramethoxysilane (TMOS), or tetraethoxysilane (TEOS) as precursors, and are dried via the supercritical drying method [7]. This method subjects the solvent in the gel to supercritical temperatures and pressures to evaporate it avoiding surface tension. While effective in minimizing shrinkage, it is expensive, energy-intensive, dangerous, and industrially challenging to optimize and upscale [8]. Alternatively, the ambient pressure drying (APD) method has been gaining scientific interest over the past decade, and protocols have been developed and optimized to produce monolithic as well as particle silica aerogel via solvent exchange with minimal shrinkage and conservation of crucial properties (high porosity, low density, low thermal conductivity) [9–12]. Indeed, as was highlighted in the work of Di Luigi et al. (2022), APD can be used to produce silica aerogel with a thermal conductivity of 23.6 mW m^{-1} K^{-1}, and porosity of 97.4 %. Sodium silicate was used as a silica source which is more sustainable than TMOS or TEOS [13].

Regarding the precursors, commercial waterglass is an alternative to organosilicates that can be used for aerogel synthesis. It is produced by

* Corresponding author.
E-mail address: m.borzova@tue.nl (M. Borzova).

https://doi.org/10.1016/j.crgsc.2024.100425
Received 27 May 2024; Received in revised form 16 July 2024; Accepted 5 August 2024
Available online 8 August 2024
2666-0865/© 2024 Published by Elsevier B.V. This is an open access article under the CC BY-NC-ND license (http://creativecommons.org/licenses/by-nc-nd/4.0/).

Table 1
Oxide composition for waste glass (wt%).

Composition	Na_2O	MgO	Al_2O_3	SiO_2	K_2O	CaO	Fe_2O_3	Other	LOI[a]
Waste glass	9.1	1.1	3.8	64.4	1.4	12.0	1.3	1.3	5.6

[a] Loss on ignition.

either melting quartz with sodium carbonate at 1400 °C, or via a hydrothermal process by combining silica sand with pure sodium hydroxide in an autoclave at a pressure of 10 bar. Both these processes utilise extreme conditions, and lead to the low sustainability of the resulting sodium silicate due to high energy demands (420–1250 MJ/ton), water consumption (2–7 kg/ton), and CO_2 emissions (403–540 kg/ton) [14–16]. Therefore, developing an alternative source for sodium silicate may have a significant impact on the product price and sustainability [17,18]. Sodium silicate has numerous applications in various industries apart from the silica aerogel synthesis such as cement production [19], food preservation, or wastewater treatment [20].

Prior research successfully synthesized aerogel by extracting silica from rice husk ash, olivine, and fly ash [21–24]. Fine glass constitutes a large fraction of the municipal solid waste including mostly glass containers for daily domestic use, as well as demolition waste. While ~50 % of waste glass is recycled globally [25], 10–30 % of waste glass is landfilled because it is broken down too finely or extensively mixed [26,27]. Hence the fine fractions of mixed glass are the least likely to be recycled, making it a cheap potential precursor for silica extraction and sodium silicate production [28]. Prior research investigated the dissolution of various types of glasses in alkaline solutions, concluding that factors such as reaction time, temperature, particle size of the glass, and pH of the solution affect the dissolution efficiency [29–31]. However, no work has looked into silica extraction or synthesis of silica aerogel from waste glass. Additionally, there is a lack of information on the balance between the practical scalability and the efficiency of such reactions.

This research aims to increase the sustainability and affordability of silica aerogel, by extracting silica from fine mixed glass waste and producing silica aerogel with minimized energy and chemical demands. The objective is to optimize the parameters for potential industrial upscaling, focusing on reducing the time and resources required for the silica extraction, and producing a high-quality aerogel. Therefore, in this study, silica was first extracted from the waste mixed soda lime glass by reacting it with a strong base and purifying it. Various reaction conditions, including time, liquid-to-solid ratios, and base type, were tested to determine optimal parameters for producing sodium silicate and subsequently silica aerogel. The properties of the synthesized silica aerogel were compared with commercially available aerogel as well as a reference sample synthesized using commercial waterglass following an APD method.

2. Methods

2.1. Raw materials

Mixed soda lime glass used in this research was obtained from HEROS Sluiskil B.V., particles were on average 17 μm in size (ranging from 4 μm to 200 μm overall) and contained shredded paper and plastic from packaging which was removed by sieving the material through a 180 μm sieve. Table 1 presents the oxide composition of the glass measured by X-ray fluorescence.

Sodium hydroxide (NaOH, VWR), sodium carbonate (Na_2CO_3, VWR), hydrochloric acid (HCl, 35 %, VWR), ammonia solution (NH_4OH, 5 M, Sigma-Aldrich), ethanol absolute (CH_3CH_2OH, 100 %, VWR), n-heptane (C_7H_{16}, analytical grade, Biosolve), trimethylchlorosilane (C_3H_9SiCl, 98 %, Sigma-Aldrich), and Amberlyst 15 hydrogen form (cation exchange resin, Sigma-Aldrich) were used to prepare silica aerogel from waste glass. Sodium silicate (Na_2SiO_3, 37 %, LabShop) was used to synthesise the reference aerogel sample. Commercial aerogel (p100, Cabot) was used for quality comparison.

Table 2
Summary of reaction parameters tested for silica dissolution optimization. All reactions were conducted under 80 °C heat with all alkaline solutions being 4 M concentration.

Sample name	Liquid-to-solid ratio	Base	Time of reaction, hrs
N6-10	10	NaOH	6
N24-10	10	NaOH	24
N48-10	10	NaOH	48
N24+24-10	10	NaOH	24 + 24
N24-50	50	NaOH	24
N24-100	100	NaOH	24
NC24-10	10	NaOH/Na_2CO_3	24
NC24-50	50	NaOH/Na_2CO_3	24

2.2. Experimental procedure

2.2.1. Silica extraction and purification

The glass was combined with an alkaline solution and stirred at 600 rpm at 80 °C for 6–48 h. The resulting solution containing impure sodium silicate was filtered with a Buchner filter and the solid residue was discarded. The high pH of the solution, coupled with the high temperature of the reaction promotes silica dissolution, via the following mechanism:

$$\equiv Si - O - Si \equiv + OH^- \rightleftharpoons \equiv Si - OH + \equiv Si - O^- \quad (1)$$

$$\equiv Si - O^- + H_2O \rightleftharpoons \equiv Si - OH + OH^- \quad (2)$$

Here, the oxygen bridges are hydrolysed by the hydroxyl anions eq (1), and unsaturated $\equiv Si - O^-$ groups are protonated to form silanol groups eq (2) by water, producing a hydroxyl anion, and also opening up the glass network for further alkaline attacks [27,32].

Hydrochloric acid (9.5 M) was then added slowly to the solution while gently stirring until the pH reached 2.0–3.0 [33]. This resulted in the solidifying of silica and NaCl salt, which were filtered, and then stirred in DI water to dissolve the salt. After washing the solid residue with DI water 3–4 times until the washing liquid became clear, pure silica was collected and dried at 105° overnight. The addition of HCl was introduced to precipitate silica and remove the impurities in the sodium silicate solution. While it is potentially possible to avoid this extra step given the appropriate industrial-scaled equipment, in this method the purity and concentration of silica are strictly controlled and optimized to obtain reliable results. Upon the addition of HCl, two types of reactions of interest take place. Firstly, the metals present in the solution such as Al, Mg, etc. form soluble metal salts with Cl^- ions and remain in the solution. When pH decreases below 3, iron forms soluble $FeCl_3$ [34]. Secondly, sodium silicate is hydrolysed to form silicic acid eq (3) which then further polymerizes and precipitates eq (4).

$$Na_2SiO_3 + H_2O + HCl \rightarrow Si(OH)_4 + 2NaCl \quad (3)$$

$$n\left[Si(OH)_4 + (OH)_4Si\right] \rightarrow n[\equiv Si - O - Si \equiv] + 2nH_2O \quad (4)$$

Water acts as a hydrolysis agent in reaction (3), when sodium silicate is converted to silicic acid. However, in the second step (4) the condensation of silicic acid takes place, which then polymerizes leading to the precipitation of solid silica and here water is the product [35]. Therefore limiting the amount of water during these steps is crucial to

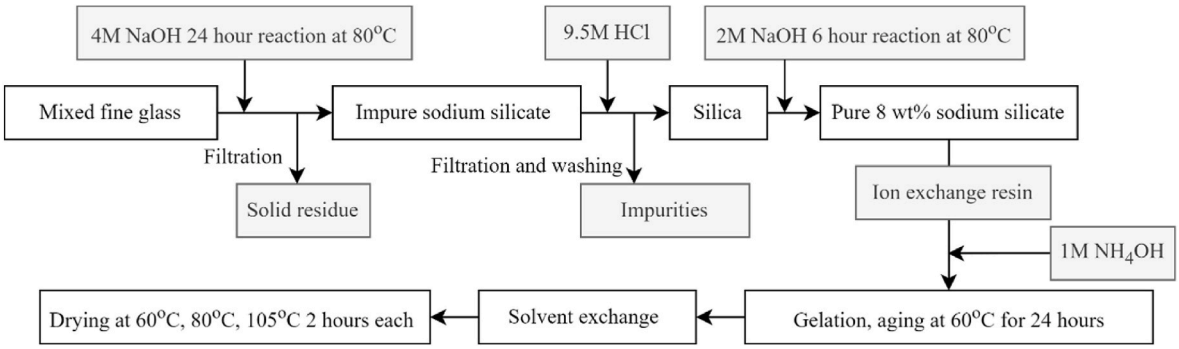

Fig. 1. Schematic representation of silica extraction from waste glass, and following silica aerogel synthesis.

Fig. 2. Photo of silica aerogel particles prepared from waste glass.

avoid tilting the balance of the reversible condensation reaction back towards monomeric silica, which is why 9.5 M of HCl was found to be ideal here for optimal extraction efficiency.

Several reaction parameters were optimized – time of reaction (6, 24, and 48 h), liquid-to-solid ratio (10, 50, and 100), and lastly the base NaOH 4 M, or 4 M 50:50 mix of NaOH/Na_2CO_3 [29]. A summary of reaction conditions for each of these processes is presented in Table 2. Weight loss (WL) was recorded by weighing the solid before and after the reaction with a base, accounting for the dissolution of the components, but also for the potential precipitation of solids. The XRF results were normalized including the weight loss and the LOI, to be able to compare the composition of solid residues with that of raw material quantitatively.

2.2.2. Silica aerogel synthesis

9 g of dry silica powder obtained from the previous silica extraction step were reacted with 8 g of NaOH in 95.5 ml of water for 6 h at 80 °C to make 8 wt% sodium silicate. It was passed through ion exchange resin and the pH dropped from 12 to 13 to 2–3 signifying the transformation of sodium silicate to silicic acid. Then 1 M solution of NH_3 was added dropwise while stirring until the pH reached 5.0–5.5, the liquid was poured into a small container and left at 60 °C overnight to age. Next, the gel was cut into pieces and solvent exchanged first with ethanol: water 1:1, followed by pure ethanol, then with ethanol:n-heptane 1:1, followed by pure n-heptane for 12 h per step. N-heptane was chosen instead of commonly used hexane due to the lower health and safety risks involved. Then a mix of TMCS:n-heptane in a 1:3 ratio was added and the gel was left at 60 °C overnight for surface modification (hydrophobicity). The unreacted TMCS and HCl that formed were removed with a pipette and the gel was once again washed with n-heptane. It was then dried at 60, 80, and 105 °C for 2 h each. The schematic representation of the reaction steps can be seen in Fig. 1, and the photo of the resulting silica aerogel can be seen in Fig. 2. It presents a slightly yellow colour due to Rayleigh scattering.

Table 3
Summary of silica aerogel samples discussed in this study, in regards to the precursor used – either sodium silicate (SS) or commercial purchase, and presence or absence of calcination at 500 °C for 4 h.

Short name	Precursor	Modifications
AG_{glass}	SS from waste glass	–
AG_{glass}-500	SS from waste glass	Calcined
AG_{ref}	Commercial SS	–
AG_{ref}-500	Commercial SS	Calcined
AG_{com}	Purchased commercially	–
AG_{com}-500	Purchased commercially	Calcined

In order to evaluate the quality of silica aerogel produced in this study, an additional aerogel was synthesized following the same method, but using commercial sodium silicate (AG_{ref}). A 37 % commercial sodium silicate was dissolved to obtain an 8 wt% silica solution (all sols having the Na:Si ratios of 2:1). Commercial silica aerogel (AG_{com}) was purchased from Cabot to complete the comparison. To investigate the effects of heat treatment on the silica aerogel network, all samples were calcined at 500 °C for 4 h (AG-500) with a heating rate of 10 °C/min. Table 3 summarizes the silica aerogel samples discussed in this study.

2.2.3. Characterization methods

To investigate the solid residue oxide composition for glass dissolution reactions X-ray Fluorescence (XRF) was performed with a PANalytical (Epsilon 3). First samples were exposed to 600 °C for 4 h to obtain a loss on ignition (LOI) value. Higher temperatures would have produced a more precise LOI, but since soda lime glass has a glass transition temperature of around 700 °C, recovering the samples from a crucible was not feasible after exposure to higher temperatures. Next, the solid sample was combined with 67 % $Li_2B_4O_7$ - 33 % $LiBO_2$ anhydrous (grade pure, Malvern Panalytical) in a 1:10 ratio, and 170 μl of 2 M LiBr were added to make the fused beads. Crystaline phases of the solid residues were identified with X-ray diffraction (XRD) using the X-ray diffractometer D2 Endeavor (Co tube, 40 kV, 30 mA, 5-70°, 0.02°/step, 0.2°/min, fixed divergence slits). The ICSD reference codes for structures identified in the samples are the following: Quartz 00-046-1045, Sodalite 00-037-0476, Natrite 00-037-0451, Calcite 01-086-2340, Sodium Aluminum Silicate 00-046-0566, Chabazite 01-085-1046.

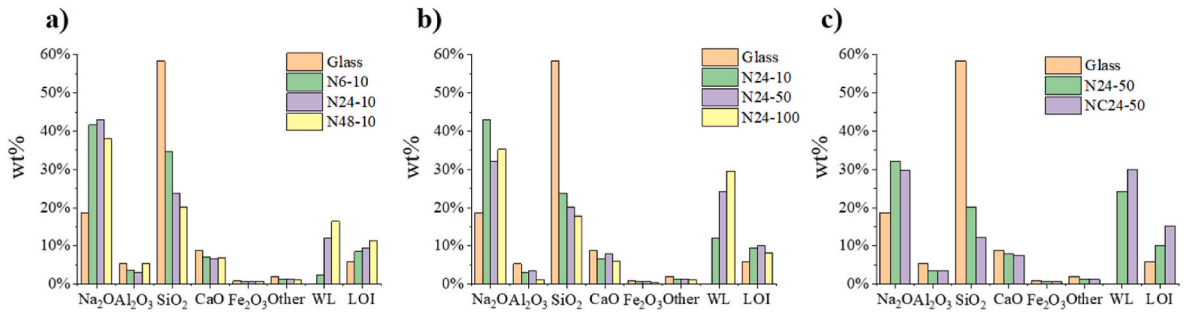

Fig. 3. X-ray fluorescence oxide compositions of silica dissolution residues compared by a) time of reaction, b) liquid-to-solid ratio, c) alkaline solution composition. Weight loss (WL) refers to the difference in mass of raw material and recovered reacted residue.

To investigate the dissolution of glass, the liquid sample was taken from the N24-10 sample each hour and analysed with ICP/OES (Inductive coupled plasma, Optical emission spectroscopy, Spectroblue FMX36 from Spectro). External (multi) standards were used for quantification. Certified reference materials from Certipur: Multistandard IV (1.11355), multi-standard XVI (1.09487), and Si standard (1.70365) were used. If those elements were present in both multi-standards, standard IV was used for calibration.

The morphology of the solid residue was investigated with Scanning Electron Microscopy (SEM) (Phenom Pro X, ThermoFisher) at 15 kV. Prior to the measurement, all samples were coated with gold (Q150T Plus, Quorum) for 50 s with a sputter current set at 30 mA. Silica aerogel samples were analysed with a Quanta 3D FEG at 15 kV.

Chemical bonds were investigated using Fourier-transform infrared spectroscopy (FTIR) on a Frontier Spectrometer from PerkinElmer in a range from 4000 cm^{-1} to 400 cm^{-1}, with 15 scans for each measurement. ^{29}Si NMR was performed using a 400 MHz Bruker machine. Relaxation time was set to 5 s for increased precision, and 1024 scans were taken. The specific surface area was measured using the BET theory, and pore size distribution using the BJH theory. Measurements were done with the nitrogen physisorption equipment Tristar II at 77 K, samples were prepared by being heated to 250 °C for 4 h to remove any residing moisture at the heating rate of 10 °C/min.

To determine the hydrophobicity of silica aerogel samples, water contact angle measurements were conducted with a Dataphysics Contact Angle System. Samples were milled and evenly distributed on a glass slide covered with a double-sided tape. A water droplet from Milli-Q with a volume of 10 μl was placed on the sample, and the contact angle was calculated.

Thermal conductivity values were obtained with the Hot Disk Thermal Constants Analyser (TPS 2500 S) at a temperature of 21 °C. Aerogel particles were placed in a plastic bag and the 7577F1 sensor was placed in the middle. A plastic bag was chosen as it achieved the best particle packing and most reliable results. Measurement permutability was set to 4 mm, the time of measurement was 10 s at 5 mW, it was repeated three times and the average was taken as a result. The range of calculation was chosen to reflect the most stable segment of the data with the lowest possible standard deviation (less than 1 mK) which was found to be 90–170 ms. The thermal stability of aerogels was analysed with a thermogravimetric analyser (TA instruments, TGA550). The heating rate was set to 5 °C/min under N_2/O_2 atmosphere up to 900 °C under room temperature of 21 °C. Due to buoyancy effects caused by the very low density of the aerogel samples measured, the TGA graph may present with a slight (<1 wt%) increase in mass at high temperatures (>800 °C) which was accounted for in the mass loss calculations.

Bulk density ρ_b of silica aerogel was calculated by measuring the volume and mass of a sample precisely by placing it in a syringe and ensuring the most efficient particle packing. Porosity Φ_a was calculated using the formula

$$\Phi_a = \left(1 - \frac{\rho_b}{\rho_s}\right) \times 100\%$$

Where ρ_s stands for skeletal density which was measured with a Helium pycnometer (AccuPyc II 1340 Micromeritics). All calcined aerogel samples were dried at 105 °C overnight before the pycnometry measurements to remove any water from the network.

3. Results and discussion

3.1. Parameter optimization for silica extraction and purification

Fig. 3 shows the composition of the solid residues after reacting the glass with an alkaline solution under various conditions. Dissolution of silica increased with time, but the relation was not linear – taking a 48-h reaction as an example the total amount of dissolved silica was 65.4 wt% (Table 4). A saturation dependency trend was observed for the time of reaction optimization (Fig. 3 a). During the first 6 h of reaction 40.7 wt% of this silica was dissolved, followed by an additional 18.4 wt% in the next 18 h, and for the final 24 h only 6.3 wt% of dissolution occurred. A potential strategy to increase the dissolution efficiency may involve conducting two consecutive 24-h reactions (N24+24-10) with a washing step in between instead of a single 48-h reaction (N48-10). Removing the dissolved silica from the solution and subjecting the residue to another reaction should increase dissolution by lowering the saturation of the reaction. This was tested, and a 48-h reaction resulted in a dissolution of 65.4 wt% of the total silica in the waste glass, while two consecutive 24-h reactions achieved 80.3 wt% dissolution, increasing silica dissolution during the last 24 h from the abovementioned 6.3 wt% in N48-10 to 21.2 wt% in N24+24-10.

Similarly, higher liquid-to-solid ratios increased the reaction efficiency for all samples (Fig. 3 b). As such, during the N24-10 reaction 59.1 % of silica was dissolved, while a ten times increase in the liquid-to-solid ratio in the N24-100 reaction resulted in 69.4 % of dissolved silica. Therefore, it was concluded that a higher liquid-to-solid ratio has little additional benefit to the reaction efficiency. A mix of $NaOH/Na_2CO_3$

Table 4
Summary of the waste glass silica dissolution in base parameter optimization. All reactions were performed at 80 °C in the same setup and environment. Amounts of silica dissolved are represented in wt%.

Parameter	Reaction time, hours				Liquid-to-solid ratio		Base	
Sample	N6-10	N24-10	N48-10	N24+24-10	N24-50	N24-100	NC24-50	NC24-10
Silica dissolved	40.7 %	59.1 %	65.4 %	80.3 %	65.6 %	69.4 %	79.2 %	54.7 %

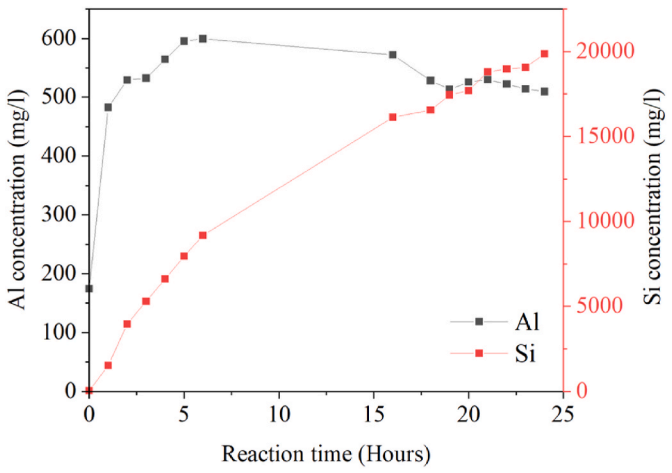

Fig. 4. Silica and alumina concentrations in the liquid phase, in mg/l, measured by ICP at the first and last 8 h of the N24-10 reaction.

with a liquid-to-solid ratio of 10 (NC24-10) showed a small decline in silica dissolution compared to the same molar concentration of NaOH (N24-10) alone (54.7 wt% and 59.1 wt% respectively). However, when reacted with NaOH/Na_2CO_3 at a liquid-to-solid ratio of 50, the amount of silica dissolved increased drastically to 79.2 wt%, indicating that the saturation of the solution at a liquid-to-solid ratio of 10 is much too high to promote silica dissolution (Table 4). While for NaOH the improvement in dissolution was lower with 59.1 wt% at 10 l:s and 65.6 % for 50 l:s. Therefore at lower saturation, the NaOH/Na_2CO_3 combination performs better than NaOH alone (Fig. 3 c). This can be due to the fact that glass contains ~8 wt% of calcium, which can deposit on the surface of the glass particles in an alkaline environment creating an inert layer of calcium silicates and preventing further silica dissolution by blocking access to the OH^- ions [36,37]. Sodium carbonate reacts with this calcite to form $CaCO_3$ and allows access to silica in the glass. An additional benefit of replacing some part of NaOH with Na_2CO_3 is that the latter is deemed to be more environmentally friendly due to the specifics of its production process [38]. While longer reaction time and higher liquid-to-solid ratio resulted in a larger yield of extracted silica, the industrial needs and possibility for upscaling were also taken into account, favouring the N24-10 reaction.

Silica dissolution efficiency was further investigated by monitoring the ionic composition of the liquid phase of the reaction for the first and last 8 h of an N24-10 reaction with ICP. This revealed that the silica dissolution commences at a high rate, which begins to decrease around the 8-h mark but does not reach complete saturation in the given 24 h (Fig. 4). Interestingly the alumina dissolution first showed a similar trend with its dissolution peak recorded at 6 h. However, during the last 8 h of the reaction, it showed a 15 % decrease, indicating the precipitation of aluminium.

XRD analysis on the solid residue of these reactions revealed that all samples contained one or more 4A-type zeolite (Fig. 5). Of those, sodalite ($Na_4Al_3Si_3O_{12}Cl$) peaks were clear and present in all samples except N6-10 and N24-100. However, the remaining 4A-type zeolites varied among samples and exhibited broader peaks at lower intensities, indicating incomplete crystalline formation. This suggests that the decrease in Al concentration in the aqueous phase could be associated with the formation and precipitation of these zeolites. Moreover, the 24 and 48-h reactions exhibited stronger zeolite peaks, indicating their tendency to form later in the reaction process, which correlates with the decline in aluminium concentration in the last 8 h.

Zeolite formation is undesirable as it leads to the loss of soluble amorphous silica and decreases extraction efficiency [32]. To better compare the amounts of zeolites in residues, the sodalite/quartz (s/q) intensity ratio was calculated based on the highest peaks for each phase (Fig. 5, d). All samples can be assumed to have the same amount of quartz as it is present in the raw waste glass and the material was well homogenized. It is also known to be unreactive under the present conditions and can be used as an internal standard. A direct comparison of the zeolite peak intensities might not give an accurate picture due to the different weight losses in each residue. Natrite and calcite were present in all samples, originating from carbonation due to the exposure to air.

The first comparison was done on the 6, 24, and 48-h reaction residues (Fig. 5, a). A 6-h reaction did not show any sodalite peaks, unlike the 24 and 48-h reactions, where the clear increase can be seen in peak

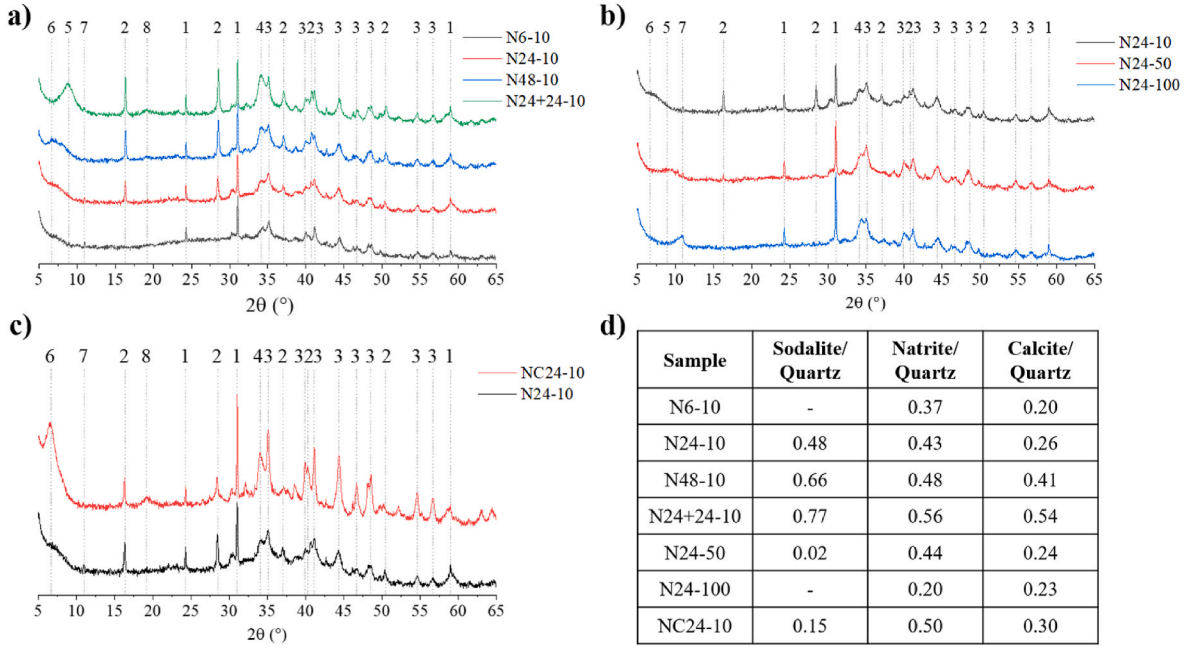

Sample	Sodalite/ Quartz	Natrite/ Quartz	Calcite/ Quartz
N6-10	-	0.37	0.20
N24-10	0.48	0.43	0.26
N48-10	0.66	0.48	0.41
N24+24-10	0.77	0.56	0.54
N24-50	0.02	0.44	0.24
N24-100	-	0.20	0.23
NC24-10	0.15	0.50	0.30

Fig. 5. X-Ray Diffraction analysis of silica dissolution residues compared by a) time of reaction, b) liquid-to-solid ratio, c) alkaline solution composition. Table d) represents the intensities ratios of the highest peaks of indicated samples. Peaks are assigned as follows: 1 – quartz, 2 – sodalite, 3 – natrite, 4 – calcite, 5 – undefined, 6 – sodium aluminum silicate, 7 – chabazite, 8 – undefined.

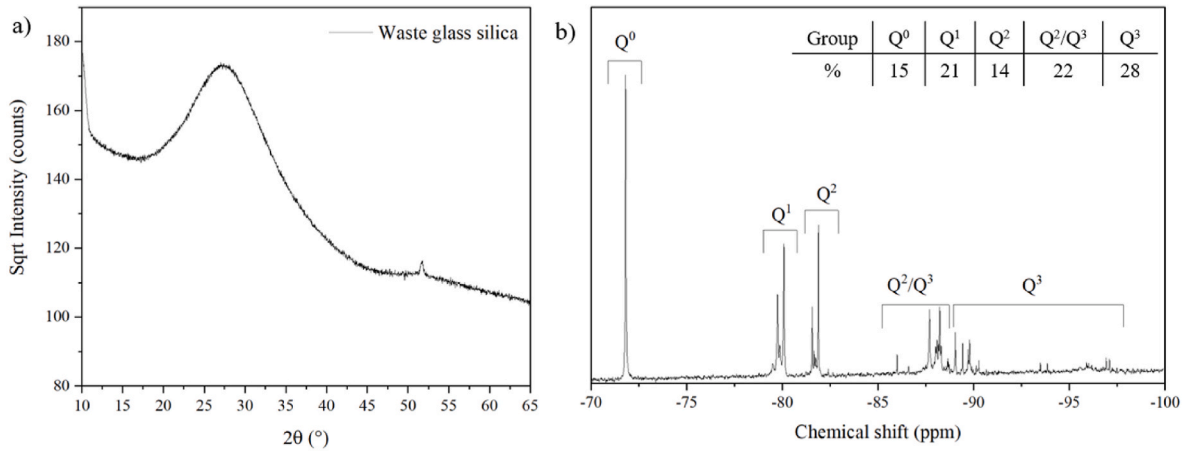

Fig. 6. a) XRD of silica produced from waste glass; b) NMR analysis on sodium silicate produced from waste glass.

intensity with an s/q ratio of 0.48 and 0.66 respectively. The dissolution of silica for the 48-h reaction was still higher despite showing more zeolite formation. In part, because zeolite formation and precipitation remove silica from the solution, therefore allowing for more amorphous silica to dissolve. Hence, while the formation of zeolites does not necessarily decrease the yield, it does result in the loss of silica that could otherwise be extracted. Comparing one 48-h reaction with two consecutive 24-h reactions showed an increase in the s/q ratio from 0.66 to 0.77. However, the XRF analysis showed much higher Si dissolution in the N24+24-10 reaction than in the N48-10. A potential reason for this difference might be the higher concentration of insoluble species in the residue, as it also shows the highest ratios of natrite and calcite to quartz. Lastly, two broad peaks with a d-spacing of 11.6 Å (5) and 5.4 Å (8) were not assigned, they may be caused by a zeolite, but their low intensity made it difficult to identify with satisfactory certainty.

Secondly, the residues with different liquid-to-solid ratios during the experiment were compared. A clear trend can be observed in Fig. 5, b. The most concentrated reaction (N24-10) indicated the highest sodalite presence, which decreased significantly for the N24-50 sample and was absent in the N24-100 one. Chabazite ($Al_{3.6}Ca_{0.18}H_{3.24}O_{24}Si_{8.4}$) was detected in all samples, albeit with a rather small peak, except for N24-100 where it was the only zeolite recorded [39].

Interestingly the alkaline solution composition affected sodalite, with NaOH being more favourable for its formation at 0.48 s/q compared to NaOH/Na_2CO_3 at s/q of 0.15. Sodium carbonate appeared to be beneficial for silica dissolution, with the only drawback being the need for a higher l:s ratio. However, XRD shows that all samples with NaOH as a base had small amounts of Na_2CO_3 in the residue, and its ratio to quartz increased with the reaction time, most likely due to the exposure to air (Fig. 5, d). This could be partially contributing to higher Si dissolution in longer reactions. Residues also showed variation in composition which can be clearly seen in the lower range of 2θ, where several zeolites were identified. Sodium Aluminum Silicate ($Al_{22.27}Na_{19.36}O_{92}Si_{73.73}$) was present in NC24-10 among others, suggesting that Na_2CO_3 as a reactant might create more favourable conditions for it when compared to samples with only NaOH used as a base. They predominantly contain sodalite [40]. Overall the majority of zeolites mentioned in this paragraph presented with rather broad peaks, and their development can be somewhat tracked when comparing e.g., the time progression of the reaction (Fig. 5, a). Since the quality of obtained silica was seemingly not affected by the dissolution parameters, the 24-h 10 liquid-to-solid ratio with NaOH base conditions were chosen for the aerogel synthesis.

Several factors are known to favour zeolite formation, such as concentration, pH, and prolonged heat exposure. In this research N24–100 and N6-10 showed the lowest presence of zeolites, therefore it can be assumed that saturation and time are major factors in silica extraction efficiency [32]. Nevertheless, some solid residue will inevitably remain, prompting this research to explore its properties and propose potential applications to prevent landfilling. While calcium deposition can be targeted by adding sodium carbonate to the base mix, which in part prevents a layer of calcite from forming on the surface of the glass particles, making the silica in it inaccessible for dissolution, calcium was still detected via EDX on the surface or within the pores of the residue.

Additionally, the SEM and optical microscopy analysis of the NC24-10 residue compared with the raw glass particles revealed that the residue has a much more uniform particle shape, with decreased geometric area (excluding pores) due to the dissolution in the base (Fig. S1). The particle size also decreased significantly, averaging from 17.4 μm in raw glass, to 12.5 μm in the residue. The residue showed a higher water retention capacity measured to be 1.87 ml/g, compared with that of 0.39 ml/g for raw glass. Furthermore, a drastic increase in the BET specific surface area was recorded at 0.61 m^2/g for raw glass and 41 m^2/g for the reacted residue (Fig. S2).

3.2. Sodium silicate analysis

An XRF analysis was performed to evaluate the purity of the precipitated silica, and excluding the LOI, 99.5 wt% SiO_2 was obtained. However, on average the LOI was measured at 20 wt%, which suggests the presence of some water in the silica. Silica obtained from olivine [23] presented an LOI of 13 wt%, so it is expected that silica retains some water. Some amount of alumina (0.4 wt%) was seen in both silica samples, which was expected since it also has a high dissolution coefficient in base and precipitates in acidic conditions. However, this value was small and its presence is not associated with any adverse effects on the quality of the produced aerogel. Higher amounts of alumina in silica may negatively influence the polymerization and strong silica network formation, so overall precautions must be taken to avoid this [41]. It was found that exposing silica powder to 9.5 M HCl at 80–100 °C for 1 h reduces the amount of alumina present by approximately half. The pH was investigated and optimized by comparing the amount of silica recovered from the filtration, as well as the purity of that silica, especially in regard to the iron salts present as they dissolve at lower pH than most other impurities [34]. In the case of this study, no significant difference in yield or purity of recovered silica was observed when precipitating at pH 1.5–4.0 for the liquid residue, therefore a pH range of 2.0–3.0 was chosen for this step.

The XRD analysis revealed the amorphous nature of silica (Fig. 6 a) with a small peak visible at a d-spacing of 2.05 Å most likely caused by a small amount of an unidentified crystalline phase. Fig. 6 b) shows the ^{29}Si NMR of sodium silicate synthesized from silica extracted from the waste glass. Peaks were assigned to each structural type, and the relative ratio of polymerized species was calculated. While peaks for Q^0

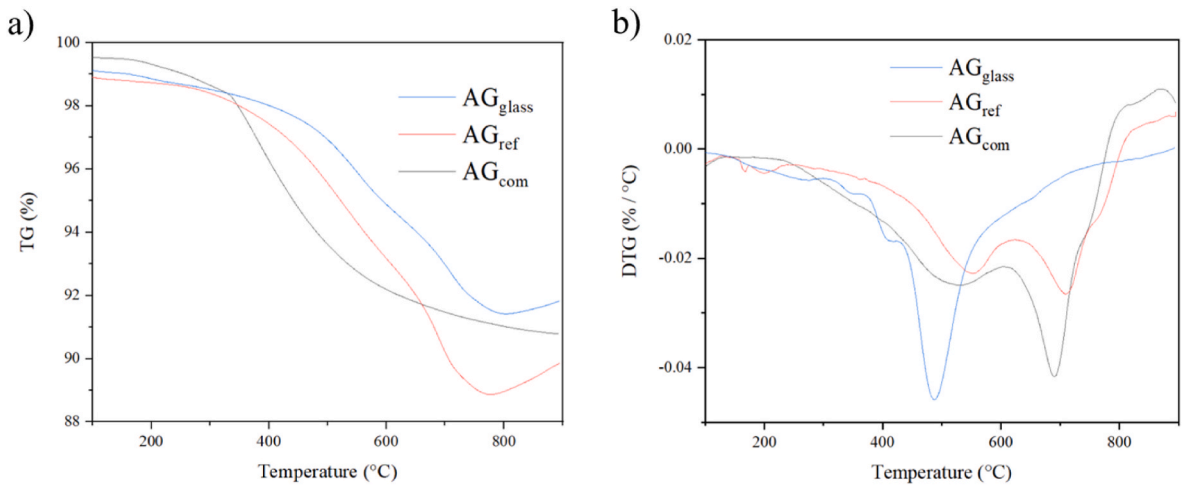

Fig. 7. Thermal stability analysis of silica aerogels a) TGA, b) DTG.

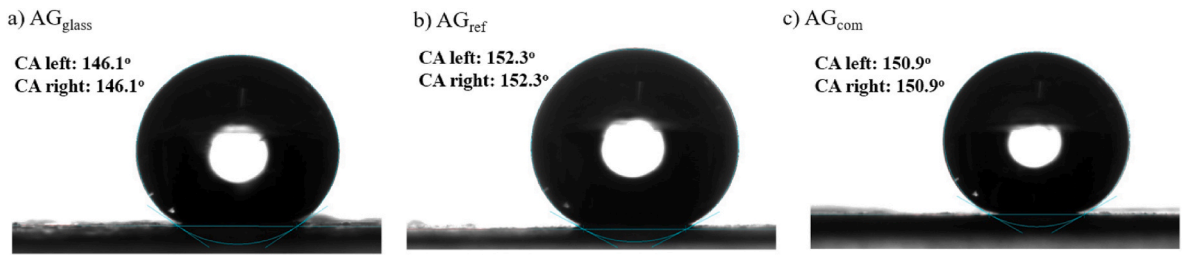

Fig. 8. The water contact angle of silica aerogel samples a) AG$_{glass}$, b) AG$_{ref}$, c) AG$_{com}$.

(monomer) and Q^1 (linear trimer) are sharp and distinct, peaks for Q^2 and Q^3 overlap in the 85–90 ppm region, hence for precision that region is assigned to a mix of both, while peaks on respective boundaries are assigned to each individually [42,43]. This overlap occurs due to the significant differences in chemical shifts for the polymerized structure caused by many potential configurations for the polymeric silicate anions, e.g. for Q^2 the following species would cause peaks in the above-mentioned region: linear trimer, linear tetramer, and mono-substituted cyclic trimer [44]. No peaks were observed for Q^4 which would be expected in the −104 to −120 ppm region [45]. This could be caused in part by the fact that species containing Q^4 are more likely to precipitate, hence they will not be detected by the liquid state NMR used here.

3.3. Silica aerogel characterization

To investigate the quality of silica aerogels and their suitability as insulation materials, characterization was carried out. The thermal conductivity of silica aerogel made from glass waste as a raw material was found to be 26 ± 0.032 mW m^{-1} K^{-1}, while commercial silica aerogel measured the same way had a thermal conductivity of 19 ± 0.021 mW m^{-1} K^{-1}.

Since this research focuses on aerogel as a building material, it is important to record the thermal stability of the product as that is crucial e.g., for fire safety. This was tested with a thermogravimetric analysis (Fig. 7). All samples showed no weight loss below 140 °C indicating that no solvent or water remained in the structure. The steep 8 % mass decrease at around 480 °C is attributed to the oxidation of the CH_3 groups on the aerogel surface from TMCS modification and the evaporation of these groups from the aerogel network [46]. Overall, aerogels remain thermally stable and hydrophobic up to 400 °C. Commercial aerogel showed a higher overall mass loss. However, the start of decomposition was not as rapid as for samples produced in this study (Fig. 7 a), which translates to two peaks visible on DTG (Fig. 7 b). This could be attributed to a different synthesis process, or the usage of other hydrophobicity agents since the water contact angle test revealed some variation between AG$_{com}$ (~151°) when compared with AG$_{glass}$ (~146°) (Fig. 8).

Table 5
Density and porosity of silica aerogels.

Sample	Skeletal density, g/cm^3	Bulk density, kg/m^3	Porosity, %
AG$_{glass}$	1.38 ± 0.0064	121.2 ± 1.9	91.2 ± 1.4
AG$_{glass}$-500	1.95 ± 0.0104	91.6 ± 1.7	95.3 ± 0.9
AG$_{ref}$	1.57 ± 0.0052	130.1 ± 3.2	91.7 ± 2.1
AG$_{ref}$-500	1.90 ± 0.0103	112.3 ± 2.8	94.1 ± 1.5
AG$_{com}$	1.47 ± 0.0091	85.2 ± 1.7	94.2 ± 1.2
AG$_{com}$-500	1.82 ± 0.0057	90.9 ± 1.9	95.0 ± 1.0

Silica aerogel was calcined at 500 °C for 4 h to investigate its effect on the structure and performance. Currently, literature reports various conclusions on the topic of heat exposure of silica aerogels. As such, research by S. He et al., reported a decrease in specific surface area after temperatures above 350 °C [47], while Y. Chen et al. observed an increase in specific surface area at 500 °C [23]. In the case of this research, calcination is seen to slightly increase the specific surface and the cumulative pore volume, while also significantly increasing the desorption average pore width from 8.3 nm in AG$_{glass}$ to 11.3 nm in AG$_{glass}$-500. Additionally, its bulk density decreases from 121.2 kg/m^3 to 91.6 kg/m^3, and its porosity increases from 91.2 % to 95.3 % (Table 5). A similar trend is observed for AG$_{ref}$ and AG$_{com}$. Such changes are attributed to the effect of methoxy group pyrolysis, which may impact the overall network structure by expanding the pores [23]. Additionally, the heat treatment-induced coarsening of the silica aerogel network would lead to an increase in skeletal density and porosity due to the increase in pore size, and reduction in the amount of micropores present. This property becomes especially relevant when further modifications are

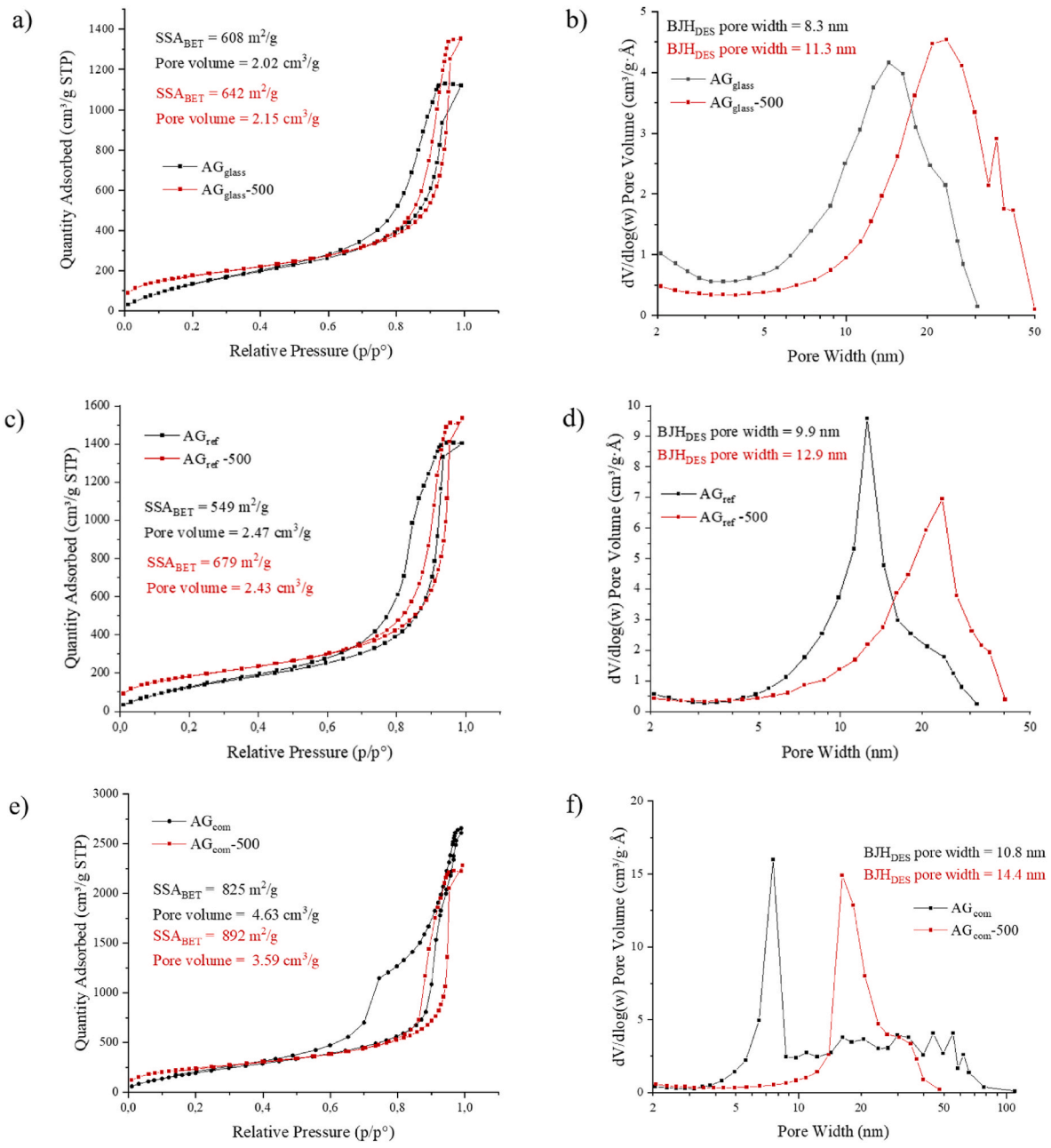

Fig. 9. a, c, e Nitrogen adsorption – desorption isotherm, specific surface area, and desorption pore volume derived by BET method; b, d, f pore size distribution and desorption pore width derived by BJH method. For aerogels produced in this study and commercial aerogel.

conducted, such as coating silica networks with additional functional groups, but would also benefit thermal insulation applications. Since temperatures above 350 °C remove organic groups of TMCS subsequently making the aerogel hydrophilic [47], in order to take advantage of these enhanced properties the surface modification would have to be repeated, which can be done via chemical vapor deposition, requiring much smaller volumes of TMCS.

Important to note, that these results can be affected by several factors: firstly, the micropores (<2 nm) could be much too small for helium molecules to enter, therefore it is possible that those are not included in the measurement of the skeletal density. Additionally, the surface of aerogel is covered with methoxy groups from TMCS surface modification, which have a lower density compared to silica and may interfere with helium penetration as well [48]. AG$_{com}$ sample showed a higher contact angle (Fig. 8a–c), as well as fewer micropores (Fig. 9b–f) when compared with AG$_{glass}$, therefore it is possible that its lower density can be in part attributed to those factors. These findings are in line with earlier studies on APD silica aerogels reporting the bulk density in the range of 80–139 kg/m^3, and porosity of 93 %–96 % [23,49,50].

BET analysis was conducted on the samples to further characterize pore morphology and aerogel network. A type H2(b) hysteresis loop was identified, which is seen in disordered materials with a wide range of pore neck sizes (e.g., ink-bottle pores) and a narrow distribution of pore cavities [51]. Such hysteresis is typical for Type IV (a) isotherms, described as having a nearly horizontal section at high p/p^0, although for mesoporous adsorbent containing macropores (>50 nm) that section is less identifiable, which can be seen in Fig. 9 for the isotherm of AG$_{glass}$ and AG$_{ref}$. A small curve at very low p/p^0 is attributed to the switch from monolayer to multilayer formation and is also a signifying part of the type IV isotherm. Aerogels produced in the scope of this research display similar isotherm behaviour and therefore similar network and pore structures. The sources of sodium silicate do not have a significant

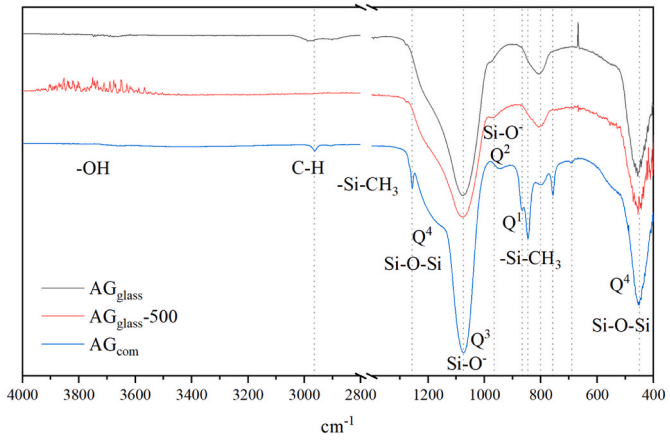

Fig. 10. Chemical bond analysis of AG_{glass}, AG_{glass}-500, and AG_{com} with FTIR.

impact on the network structures of the silica aerogels. However, AG_{glass} had a higher surface area (608 m^2/g) than AG_{ref} (549 m^2/g). The desorption cumulative volume of pores does seem to be lower for AG_{glass} than for AG_{ref} (2.02, and 2.47 cm^3/g respectively), indicating that AG_{glass} may have a higher quantity of smaller pores. In addition, the pore width distributions appear narrower for AG_{ref}, with slightly more micropores present for the AG_{glass}.

Overall, the observed variations between uncalcined aerogel samples are relatively minor and could be caused by either impurities or deviations in the preparation process. A more notable difference was seen when analysing the commercial aerogel sample. AG_{com} exhibited a rather distinct isotherm, which appears to be closer to the type III classification due to the absence of two typical features of type IV described above. Hysteresis is much more pronounced while still resembling the H2(b) type, which signifies a higher degree of pore condensation and pore blocking. Differences in adsorption and desorption average pore widths (15.2 nm and 11.8 nm respectively) also point to the fact that the sample contains many narrow-neck pores. While AG_{glass} also exhibited such structures, the difference was less pronounced – 9.0 nm for adsorption and 8.3 nm for desorption. The surface area of AG_{com} (825 m^2/g) and pore volume of 4.63 cm^3/g were notably higher than those of aerogels made in this study, which is expected when comparing a laboratory product to an industrial one. The properties of AG_{glass} are similar to those of prior studies reporting aerogel synthesized from alternative raw materials such as rice husk ash, olivine, or fly ash (SSA_{BET} = 362–946 m^2/g, pore volume = 0.74–4.88 cm^3/g) [23,49,52].

The heat treatment led to an increase in BET surface areas, desorption cumulative volumes of pores, and desorption pore widths for all samples. In AG_{com} it also narrowed the pore width distribution making it more consistent (Fig. 9 f). This is in line with the reported density and porosity improvements, leading to the conclusion that calcination enhanced the properties of aerogels produced in this study as well as the commercial sample. Prior research also reported an increase in SSA_{BET} and pore volume upon exposure to 500 °C due to the coarsening of the backbone in the silica network [23].

Chemical bond analysis was performed to further investigate the differences between the aerogels produced in this study and the commercial sample. Fig. 10 depicts the FTIR analysis of 3 samples: silica aerogel produced from silica extracted from mixed waste glass with (AG_{glass}-500) and without (AG_{glass}) calcination, and commercial silica aerogel (AG_{com}). Other aerogels produced in this study are not included since their chemical bond composition was indistinguishable from the AG_{glass} sample. TMCS peaks present in the AG_{glass} sample confirmed that the surface modification was successful, additionally supported by the absence of an -OH peak in the 3300 cm^{-1} region [53,54]. Silica network peaks are assigned according to their polymerization factor Q^1-Q^4, and if the oxygen atom is bridging (Si–*O*–Si) or non-bridging (Si–O^-) (Table 6)

Table 6
A summary of assigned FTIR peaks present in Fig. 10.

Peak range cm^{-1}	Assigned species	Vibration type
2950	C–H	Stretching
1260	Si–CH_3	Bending
1200	Si–*O*–Si (Q^4)	Stretching
1070	Si–O^- (Q^3)	Stretching
970	Si–O^- (Q^2)	Stretching
860	Si–CH_3	Stretching
800	Si–C; Si–O	Stretching
740	CH_2	Rocking
695	Si–O	Stretching
550	Si–*O*–Si	Bending
450	Si–*O*–Si (Q^4)	Rocking

[55,56]. A small Q^1 peak at around 860 is visible only for the commercial aerogel, which is potentially covered by a strong -*Si*-CH_3 band in the other two samples [56]. The peaks for TMCS are absent in AG_{glass}-500 which is expected after calcination. Overall, the presence of all the abovementioned structural species is consistent among the three samples, which points towards network similarities.

To investigate the morphology of aerogel samples and confirm the effects of calcination on the aerogel network, SEM pictures were taken (Fig. 11, Fig. S3). One interesting change that stands out is some loss of homogeneity in the calcined samples (Fig. 11c and d) when compared to the original aerogels (Fig. 11a and b). Heat exposure seems to cause some aggregation and clustering, which could be explained by the loss of micropores due to pore wall collapse, and fusion of the primary particles. This leads to another observed difference which is the increase of individual particle sizes within the aerogel network in calcined species that was seen for all samples. During the pyrolysis, the hydrophobic methyl groups on the aerogel surface undergo oxidation to form hydroxyl groups, which then condense to form Si–*O*–Si bonds, causing coarsening of the 3D network, and visible polymerization of particles [57]. At the same time the average pore width values increased among these newly formed clusters as shown previously in the BET analysis (Fig. 9). Depending on the desired properties of the aerogel, thermal treatment can be used as a means to enhance e.g., pore width and surface areas, while preserving the network intact. Previous studies have also highlighted additional advantages, including reduced thermal conductivity, showcasing the considerable potential of this method [57].

4. Conclusions

Fine fractions of mixed waste soda lime glass were used to extract silica with an alkaline solution. After a necessary purification step the extracted silica was used for synthesis of silica aerogel via the ambient pressure drying method. This aerogel was compared with commercial products, as well as with a sample made from commercial sodium silicate.

- Parameters such as time, liquid-to-solid ratio, and the base itself had a significant influence on the reaction efficiency, with 24 h, 10 l:s, and NaOH (4 M) being the most optimal when considering the balance between maximizing silica yield and minimizing the liquid-to-solid ratio and the reaction time. Longer reactions and more saturated solutions appeared to be more prone to zeolite formation, leading to the loss of amorphous silica. However, such reactions also showed a higher yield of silica.
- The resulting aerogel possessed low thermal conductivity (26 mW m−1 K−1), high specific surface area (608 m^2/g), and was hydrophobic with a water contact angle of 146.1° among other properties, making it a suitable insulation material.
- With some minor variations in values reported in this study, no significant and consistent differences were observed between waste glass and commercial sodium silicate aerogel samples, leading to a

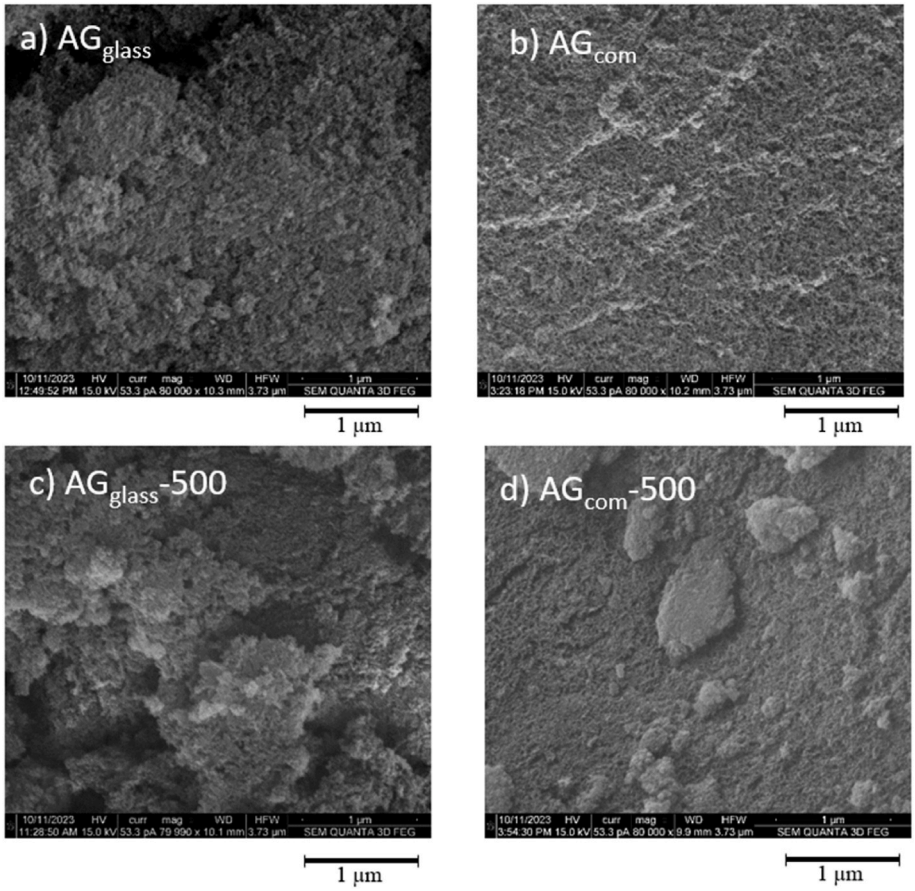

Fig. 11. SEM images of a) AG_{glass}, b) AG_{com}, c) AG_{glass}-500, d) AG_{com}-500 under magnification of 80,000.

conclusion that waste glass is a suitable raw material for aerogel synthesis. Additionally, both aerogels had comparable properties to the commercial aerogel sample.

- Heat treatment of all aerogels was investigated by subjecting the samples to 500 °C for 4 h, to explore the route for further surface modifications or property enhancements. Their behaviour was very similar, presenting higher surface areas, and lower micropore count among other characteristics after calcination. Therefore, opening a potential possibility for targeted property improvements after the drying step.

Overall, waste glass is a promising raw material for silica aerogel production and can be combined with a low-energy drying method to decrease the associated economic costs, as well as to increase its sustainability. This makes it a compelling candidate for large-scale use as a housing insulation material. However, the main limitation of this study is the lack of data to ensure the environmental benefits of the proposed method. Further investigation is needed to quantify the sustainability of this process through a Life Cycle Assessment to ensure scalability and compare it with the current production methods. Further optimization of the process would also be beneficial to minimize the time of the synthesis as well as the resources used. Additionally, exploring the recycling of the unreacted glass residue from silica extraction for example as a supplementary cementitious material would reduce the overall waste.

CRediT authorship contribution statement

M. Borzova: Conceptualization, Data curation, Formal analysis, Investigation, Methodology, Validation, Visualization, Writing – original draft, Writing – review & editing. **K. Schollbach:** Conceptualization, Supervision, Writing – review & editing. **F. Gauvin:** Conceptualization, Supervision, Writing – review & editing. **H.J.H. Brouwers:** Funding acquisition, Project administration, Resources, Supervision.

Declaration of competing interest

The authors declare that they have no known competing financial interests or personal relationships that could have appeared to influence the work reported in this paper.

Data availability

Data will be made available on request.

Acknowledgement

This research is funded by project BRIMM (Bright Renovatie Isolatie voor woningschil door (Advanced) Materialen en Methodes) under Missiegedreven Onderzoek, Ontwikkeling en Innovatie (MOOI). The authors acknowledge Beatrice Cerrai for assistance with SEM measurements.

Appendix A. Supplementary data

Supplementary data to this article can be found online at https://doi.org/10.1016/j.crgsc.2024.100425.

References

[1] Eurostat. Energy Data. https://ec.europa.eu/eurostat/web/energy/data (accessed 2023-February-22).

[2] Klimaat-akkord. Agreements for Built Environment. https://www.klimaatakkoord.nl/gebouwde-omgeving.

[3] Z. Li, X. Cheng, L. Gong, Q. Liu, S. Li, Enhanced flame retardancy of hydrophobic silica aerogels by using sodium silicate as precursor and phosphoric acid as catalyst, J. Non-Cryst. Solids 481 (2018) 267–275, https://doi.org/10.1016/J.JNONCRYSOL.2017.10.053.

[4] A.V. Rao, G.M. Pajonk, D. Haranath, Synthesis of hydrophobic aerogels for transparent window insulation applications, Material Sci. Technol. 17 (3) (2013) 343–348, https://doi.org/10.1179/026708301773002572.

[5] L.D. Hung Anh, Z. Pásztory, An overview of factors influencing thermal conductivity of building insulation materials, J. Build. Eng. 44 (2021) 102604, https://doi.org/10.1016/J.JOBE.2021.102604.

[6] C. Thie, S. Quallen, A. Ibrahim, T. Xing, B. Johnson, Study of energy saving using silica aerogel insulation in a residential building, Gels 9 (2) (2023), https://doi.org/10.3390/gels9020086.

[7] M.A. Aegerter, N. Leventis, M.M. Koebel, Aerogels Handbook, Springer, New York, 2011.

[8] M. Dowson, M. Grogan, T. Birks, D. Harrison, S. Craig, Streamlined Life Cycle assessment of transparent silica aerogel made by supercritical drying, Appl. Energy 97 (2012) 396–404, https://doi.org/10.1016/J.APENERGY.2011.11.047.

[9] S.W. Hwang, T.Y. Kim, S.H. Hyun, Effect of surface modification conditions on the synthesis of mesoporous crack-free silica aerogel monoliths from waterglass via ambient-drying, Microporous Mesoporous Mater. 130 (1–3) (2010) 295–302, https://doi.org/10.1016/J.MICROMESO.2009.11.024.

[10] C.E. Kim, J.S. Yoon, H.J. Hwang, Synthesis of nanoporous silica aerogel by ambient pressure drying, J. Sol. Gel Sci. Technol. 49 (1) (2009) 47–52, https://doi.org/10.1007/S10971-008-1828-7/FIGURES/6.

[11] S.-W. Hwang, H.-H. Jung, S.-H. Hyun, Y.-S. Ahn, Effective preparation of crack-free silica aerogels via ambient drying, J. Sol. Gel Sci. Technol. 41 (2) (2006) 139–146, https://doi.org/10.1007/S10971-006-0513-Y, 2007.

[12] S.D. Bhagat, Y.H. Kim, Y.S. Ahn, J.G. Yeo, Textural properties of ambient pressure dried water-glass based silica aerogel beads: one day synthesis, Microporous Mesoporous Mater. 96 (1–3) (2006) 237–244, https://doi.org/10.1016/J.MICROMESO.2006.07.002.

[13] M. Di Luigi, Z. Guo, L. An, J.N. Armstrong, C. Zhou, S. Ren, Manufacturing silica aerogel and cryogel through ambient pressure and freeze drying, RSC Adv. 12 (33) (2022) 21213–21222, https://doi.org/10.1039/D2RA03325A.

[14] M. Fawer, M. Concannon, W. Rieber, Life Cycle inventories for the production of sodium silicates, Int. J. Life Cycle Assess. 4 (4) (1999) 207–212, https://doi.org/10.1007/BF02979498/METRICS.

[15] X. Gao, Q.L. Yu, A. Lazaro, H.J.H. Brouwers, Investigation on a green olivine nano-silica source based activator in alkali activated slag-fly ash blends: reaction kinetics, gel structure and carbon footprint, Cement Concr. Res. 100 (2017) 129–139, https://doi.org/10.1016/J.CEMCONRES.2017.06.007.

[16] European Comission, Reference Document on Best Available Techniques for the Manufacture of Large Volume Inorganic Chemicals – Solids and Others Industry, 2007.

[17] M. Dowson, M. Grogan, T. Birks, D. Harrison, S. Craig, Streamlined Life Cycle assessment of transparent silica aerogel made by supercritical drying, Appl. Energy 97 (2012) 396–404, https://doi.org/10.1016/j.apenergy.2011.11.047.

[18] F. Andreola, L. Barbieri, I. Lancellotti, The environmental friendly route to obtain sodium silicate solution from rice husk ash: a comparative study with commercial silicates deflocculating agents, Waste Biomass Valorization 11 (11) (2020) 6295–6305, https://doi.org/10.1007/S12649-019-00849-W/FIGURES/8.

[19] V.D. Glukhowsky, Slag–alkali concretes produced from fine-grained aggregates, Vishcha Shkola 223 (1981).

[20] G. Lagaly, W. Tufar, A. Minihan, A. Silicates Lovell, Ullmann's Encyclopedia of Industrial Chemistry, 2000, https://doi.org/10.1002/14356007.A23_661.

[21] N. Karamahmut Mermer, S. Piskin, Silica based aerogel synthesis from fly ash and bottom ash: the effect of synthesis parameters on the structure, Main Group Chem. 17 (1) (2018) 63–77, https://doi.org/10.3233/MGC-180254.

[22] Y. Cheng, M. Xia, F. Luo, N. Li, C. Guo, C. Wei, Effect of surface modification on physical properties of silica aerogels derived from fly ash acid sludge, Colloids Surf. A Physicochem. Eng. Asp. 490 (2016) 200–206, https://doi.org/10.1016/J.COLSURFA.2015.11.055.

[23] Y.X. Chen, Y. Hendrix, K. Schollbach, H.J.H. Brouwers, A silica aerogel synthesized from olivine and its application as a photocatalytic support, Construct. Build. Mater. 248 (2020) 118709, https://doi.org/10.1016/J.CONBUILDMAT.2020.118709.

[24] J.P. Nayak, J. Bera, Preparation of silica aerogel by ambient pressure drying process using rice husk ash as raw material, Trans. Indian Ceram. Soc. 68 (2) (2009) 91–94, https://doi.org/10.1080/0371750X.2009.11082163.

[25] W. Ran, F. Chen, Q. Wu, S. Liu, A study of the closed-loop supply chain coordination on waste glass bottles recycling, Math. Probl Eng. 2016 (2016), https://doi.org/10.1155/2016/1049514.

[26] Larsen, A. W.; Merrild, H.; Christensen, T. H. Recycling of Glass: Accounting of Greenhouse Gases and Global Warming Contributions. https://doi.org/10.1177/0734242X09342148.

[27] M. Torres-Carrascoa, J.G. Palomob, F. Puertasa, View of sodium silicate solutions from dissolution of glasswastes. Statistical analysis, Mater. Construcción 64 (314) (2014).

[28] M. Dathe, H. Roggendorf, Dissolution of sodium silicate glasses for the production of water glass – Part I: study of experimental parameters, Eur. J. Glasses Sci. Technol. B Phys. Chem. Glasses 59 (5) (2018) 241–250, https://doi.org/10.13036/17533562.59.5.006.

[29] M. Torres-Carrascoa, J.G. Palomob, F. Puertasa, View of sodium silicate solutions from dissolution of glasswastes. Statistical analysis, Mater. Construcción 64 (314) (2014).

[30] A. Elia, K. Ferrand, K. Lemmens, Determination of the forward dissolution rate for international simple glass in alkaline solutions, MRS Adv 2 (12) (2017) 661–667, https://doi.org/10.1557/ADV.2016.672.

[31] S. Rossignol, S.S. Kouassi, J. Andji, J.-P. Bonnet, Dissolution of waste glasses in high alkaline solutions, Original papers Ceramics-Silikáty 54 (3) (2010) 235–240.

[32] Q. Alam, Y. Hendrix, L. Thijs, A. Lazaro, K. Schollbach, H.J.H. Brouwers, Novel low temperature synthesis of sodium silicate and ordered mesoporous silica from incineration bottom ash, J. Clean. Prod. 211 (2019) 874–883, https://doi.org/10.1016/J.JCLEPRO.2018.11.173.

[33] J. Xiao, F. Li, Q. Zhong, H. Bao, B. Wang, J. Huang, Y. Zhang, Separation of aluminum and silica from coal gangue by elevated temperature acid leaching for the preparation of alumina and SiC, Hydrometallurgy 155 (2015) 118–124, https://doi.org/10.1016/J.HYDROMET.2015.04.018.

[34] R. Pirie, D. Batstone, Alkaline Digestion of Glass. CN113195425A, 2019.

[35] I. Made Joni, Rukiah, C. Panatarani, Synthesis of silica particles by precipitation method of sodium silicate: effect of temperature, PH and mixing technique, in: AIP Conf Proc, 2219, 2020 80018, https://doi.org/10.1063/5.0003074.

[36] H. Maraghechi, F. Rajabipour, C.G. Pantano, W.D. Burgos, Effect of calcium on dissolution and precipitation reactions of amorphous silica at high alkalinity. https://doi.org/10.1016/j.cemconres.2016.05.004, 2016.

[37] Y. Oka, K.S. Ricker, M. Tomozawa, Calcium deposition on glass surface as an inhibitor to alkaline attack, J. Am. Ceram. Soc. 62 (11–12) (1979) 631–632, https://doi.org/10.1111/j.1151-2916.1979.tb12751.x.

[38] A. Adesina, Performance and sustainability overview of sodium carbonate activated slag materials cured at ambient temperature, Resources, Environment and Sustainability 3 (2021) 100016, https://doi.org/10.1016/J.RESENV.2021.100016.

[39] K. Soga, H. Imamura, S. Ikeda, W.J. Mortler, G.S. D King, L. Sengler, Crystal structures of dehydrated H chabazite crystal structures of dehydrated H chabazite pretreated at 320 °C, and at 600 °C after steaming, J. Phys. Chem. A 81 (9) (1977) 4910.

[40] anL. Lievens, J.P. Verduijn, A.-J. Bons, W.J. ortier, Cation Site Energies in Dehydrated Hexagonal Faujasite (EMT), 1992.

[41] L. Lunevich, P. Sanciolo, A. Smallridge, S.R. Gray, Silica scale formation and effect of sodium and aluminium ions - 29 Si NMR study, Environ. Sci. 2 (1) (2016) 174–185, https://doi.org/10.1039/C5EW00220F.

[42] H. Jansson, D. Bernin, K. Ramser, Silicate species of water glass and insights for alkali-activated green cement, AIP Adv. 5 (6) (2015) 067167, https://doi.org/10.1063/1.4923371.

[43] S. Sjöberg, Silica in aqueous environments, J. Non-Cryst. Solids 196 (1996) 51–57, https://doi.org/10.1016/0022-3093(95)00562-5.

[44] T. Hiemstra, W.H. van Riemsdijk, Multiple activated complex dissolution of metal (hydr) oxides: a thermodynamic approach applied to quartz, J. Colloid Interface Sci. 136 (1) (1990) 132–150, https://doi.org/10.1016/0021-9797(90)90084-2.

[45] A. Borba, J.P. Vareda, L. Durães, A. Portugal, P.N. Simões, Spectroscopic characterization of silica aerogels prepared using several precursors – effect on the formation of molecular clusters, New J. Chem. 41 (14) (2017) 6742–6759, https://doi.org/10.1039/C7NJ01082F.

[46] J.L. Gurav, A.V. Rao, A.P. Rao, D.Y. Nadargi, S.D. Bhagat, Physical properties of sodium silicate based silica aerogels prepared by single step sol–gel process dried at ambient pressure, J. Alloys Compd. 476 (1–2) (2009) 397–402, https://doi.org/10.1016/J.JALLCOM.2008.09.029.

[47] S. He, Y. Huang, G. Chen, M. Feng, H. Dai, B. Yuan, X. Chen, Effect of heat treatment on hydrophobic silica aerogel. https://doi.org/10.1016/j.jhazmat.2018.08.087, 2018.

[48] A. Ayral, J. Phalippou, T. Woignier, Skeletal density of silica aerogels determined by helium pycnometry, J. Mater. Sci. 27 (5) (1992) 1166–1170, https://doi.org/10.1007/BF01142014.

[49] Q. Feng, K. Chen, D. Ma, H. Lin, Z. Liu, S. Qin, Y. Luo, Synthesis of high specific surface area silica aerogel from rice husk ash via ambient pressure drying, Colloids Surf. A Physicochem. Eng. Asp. 539 (2018) 399–406, https://doi.org/10.1016/J.COLSURFA.2017.12.025.

[50] F. Shi, L. Wang, J. Liu, Synthesis and characterization of silica aerogels by a novel fast ambient pressure drying process, Mater. Lett. 60 (29–30) (2006) 3718–3722, https://doi.org/10.1016/J.MATLET.2006.03.095.

[51] M. Thommes, K.A. Cychosz, Physical adsorption characterization of nanoporous materials: progress and challenges, Adsorption 20 (2–3) (2014) 233–250, https://doi.org/10.1007/S10450-014-9606-Z/FIGURES/11.

[52] F. Shi, J.X. Liu, K. Song, Z.Y. Wang, Cost-effective synthesis of silica aerogels from fly ash via ambient pressure drying, J. Non-Cryst. Solids 356 (43) (2010) 2241–2246, https://doi.org/10.1016/J.JNONCRYSOL.2010.08.005.

[53] M. aki Muroya, Correlation between the formation of silica skeleton structure and fourier transform reflection infrared absorption spectroscopy spectra, Colloids Surf. A Physicochem. Eng. Asp. 157 (1–3) (1999) 147–155, https://doi.org/10.1016/S0927-7757(99)00054-0.

[54] S. He, D. Huang, H. Bi, Z. Li, H. Yang, X. Cheng, Synthesis and characterization of silica aerogels dried under ambient pressure bed on water glass, J. Non-Cryst. Solids 410 (2015) 58–64, https://doi.org/10.1016/J.JNONCRYSOL.2014.12.011.

[55] B.O. Mysen, J.D. Frantz, B.O. Mysen, J.D. Frantz, Silicate melts at magmatic temperatures: in-situ structure determination to 1651 ~ C and effect of temperature and bulk composition on the mixing behavior of structural units, Contrib. Mineral. Petrol. 117 (1994) 1–14.

[56] J. Tan, S. Zhao, W. Wang, G. Davies, X. Mo, The effect of cooling rate on the structure of sodium silicate glass, Mater Sci Eng B Solid State Mater Adv Technol 106 (3) (2004) 295–299, https://doi.org/10.1016/J.MSEB.2003.09.045.

[57] Z. Lun, L. Gong, Z. Zhang, Y. Deng, Y. Zhou, Y. Pan, X. Cheng, Improvement of the thermal insulation performance of silica aerogel by proper heat treatment: microporous structures changes and pyrolysis mechanism, Gels 8 (3) (2022), https://doi.org/10.3390/gels8030141.